American Mineralogist, Volume 94, pages 666–675, 2009

Arsenate substitution in hydroxylapatite: Structural characterization of the $Ca_5(P_xAs_{1-x}O_4)_3OH$ solid solution

YOUNG J. LEE,[1] PETER W. STEPHENS,[2] YUANZHI TANG,[3] WEI LI,[3] BRIAN L. PHILLIPS,[3] JOHN B. PARISE,[3,4] AND RICHARD J. REEDER[3,*]

[1]Department of Earth and Environmental Sciences, Korea University, Seoul 136-701, Korea
[2]Department of Physics and Astronomy, Stony Brook University, Stony Brook, New York 11794, U.S.A.
[3]Department of Geosciences and Center for Environmental Molecular Science, Stony Brook University, Stony Brook, New York 11794, U.S.A.
[4]Department of Chemistry, Stony Brook University, Stony Brook, New York 11794, U.S.A.

ABSTRACT

Arsenate (As^{5+}) substitution in the hydroxylapatite structure was examined using a combination of crystallographic and spectroscopic techniques. Samples of hydroxylapatite, the As^{5+}-substituted analog (synthetic johnbaumite), and five intermediate compositions were synthesized from solution. Synchrotron X-ray diffraction data show that all samples are single-phase, confirming complete substitution. No evidence is found for lowering of symmetry below $P6_3/m$. Rietveld structure refinements show progressive expansion of the unit cell with increasing As substitution, which can be accounted for primarily by an average expansion of the tetrahedral site. Sizes of Ca polyhedra show little variation as a result of As substitution. NMR results show no evidence for local clustering of PO_4 tetrahedra. EXAFS confirms that the size of As-centered tetrahedra remains constant across the solid-solution series.

Keywords: Apatite, hydroxylapatite, johnbaumite, arsenic, arsenate, NMR, EXAFS

INTRODUCTION

Occurrences of dissolved As in surface and ground waters and observed adverse health effects have emphasized the need for better understanding of reactions that govern As mobility in the environment. Arsenic is commonly released to aqueous solutions by oxidative weathering of arsenides and reduced As in ore minerals and by dissolution of arsenite and arsenate minerals formed in oxidation zones of ore bodies. Release of As species sorbed onto mineral surfaces is also recognized as a source of dissolved As. Anthropogenic sources may also be important locally. Incorporation of As in precipitating phases is one of the dominant strategies for its removal from water. The effectiveness of this sequestration approach depends on the solubility and stability of the As-containing phase. Solubilities of As^{3+} and As^{5+} minerals vary widely, and As^{3+} and As^{5+} aqueous species, dominantly oxyanions, may be mobile in surface waters depending on redox and pH conditions. Much attention has been given to methods for removal of dissolved As from wastewaters associated with mining activities (Robins 1985; Nishimura and Robins 1998; Donahue and Hendry 2003) and from drinking water (Mondal et al. 2006; Choong et al. 2007). In the case of As^{5+}-containing waters, addition of lime has been used widely to induce precipitation of calcium arsenate phases. Despite the overall effectiveness of this method, studies have shown that solubilities of some initially formed calcium arsenates are not sufficiently low to limit dissolved arsenate concentrations within water quality guidelines (Robins 1981). In addition, the high pH values caused by lime addition favor uptake of atmospheric CO_2 over time, which has been shown to result in conversion of some initially formed calcium arsenate phases to calcium carbonate, accompanied by release of As (Robins 1985). Nevertheless, precipitation of calcium arsenate phases remains a widely used method for limited removal of As from waste and drinking waters and may control dissolved arsenate concentrations in some natural waters.

Nishimura and Robins (1998) and Bothe and Brown (1999a, 1999b) conducted extensive synthesis experiments at ambient temperatures to evaluate the conditions of formation and solubilities of different calcium arsenates. Their results demonstrated that different phases form, depending on subtle variations in synthesis conditions. The formation products varied in Ca/As stoichiometry, degree of hydration, and solubility. Several groups (Bothe and Brown 1999a, 1999b; Massuyes et al. 1969; Mahapatra et al. 1987; Myneni et al. 1997, 1998; Moon et al. 2004; Zhu et al. 2006) have synthesized the phase $Ca_5(AsO_4)_3OH$, which corresponds to the mineral johnbaumite, first described by Dunn et al. (1980). This mineral phase is the arsenate analog of hydroxylapatite, $Ca_5(PO_4)_3OH$, as well as the hydroxyl analog of svabite, $Ca_5(AsO_4)_3F$. Because hydroxylapatite (HAP) is the most stable form of calcium phosphate and exhibits a moderately low solubility, Nishimura and Robins (1998) speculated that the arsenate analog, $Ca_5(AsO_4)_3OH$, designated hereafter as AsHAP, is also likely to exhibit a low solubility, and therefore may be effective in limiting dissolved arsenate concentrations. Experimental studies, however, have demonstrated that the solubility of AsHAP is significantly greater than that of HAP (Bothe and Brown 1999b; Mahapatra et al. 1987; Myneni et al. 1997; Zhu et

* E-mail: rjreeder@stonybrook.edu

0003-004X/09/0506–666$05.00/DOI: 10.2138/am.2009.3120

al. 2006). Magalhaes and Williams (2007) suggested that phosphate substitution in the arsenate compound could significantly reduce its solubility.

The presence of dissolved phosphate in many natural settings raises the possibility that phases intermediate in composition between $Ca_5(PO_4)_3OH$ and $Ca_5(AsO_4)_3OH$ may form in preference to end-member compositions. Massuyes et al. (1969) describe experimental syntheses of the complete $Ca_5(P_xAs_{1-x}O_4)_3OH$ solid solution. Synthesis experiments conducted by Bothe and Brown (1999a) failed to produce sample compositions spanning the complete solid solution. They found that formation of nearly pure AsHAP was favored over a broad range of As/P solution ratios. Their synthesis method involved reaction of high-purity $Ca(OH)_2$(s) with arsenate- and phosphate-containing solutions at room temperature. Results of experiments utilizing a different synthesis method indicate that compositions across the complete solid-solution series can be readily synthesized at 100 °C and at ambient temperature (U.S. Environmental Protection Agency 1998). This suggests that the compositional range of synthesis products depends on the method used. Complete PO_4-AsO_4 substitution has also been demonstrated in experimental studies of apatite analogs, such as in the system $Sr_5(PO_4)_3OH$-$Sr_5(AsO_4)_3OH$ (George et al. 1987).

The apatite structure is well known for accommodating a wide range of chemical substitutions, which may occur at two positions normally occupied by Ca, A1 and A2 (or Ca1 and Ca2), the tetrahedral B position, or in the column anion site, X. White and Dong (2003) have attributed the diverse range of possible cation substitutions to the inherent flexibility of the corner-connected A1-BO_4 framework that circumscribes the one-dimensional tunnels containing the A2-X components. Whereas the prototype structure has hexagonal symmetry ($P6_3/m$), ordering and/or distortions can reduce symmetry to monoclinic or triclinic in some examples (Baikie et al. 2007).

For the present study, we have synthesized single-phase samples having the apatite structure and spanning the complete solid-solution series $Ca_5(PO_4)_3OH$-$Ca_5(AsO_4)_3OH$. The focus of this paper is characterization of their structural properties using X-ray diffraction (XRD), Fourier transform infrared spectroscopy (FTIR), extended X-ray absorption fine structure (EXAFS), nuclear magnetic resonance (NMR), and thermogravimetric analysis (TGA). In particular, we report Rietveld structure refinement results for samples across the complete solid solution, including pure AsHAP, revealing the structural variation associated with AsO_4 substitution in hydroxylapatite.

Experimental methods

Synthesis methods

Two different solution growth methods were explored for synthesizing samples. The method that produced samples having better crystallinity for X-ray diffraction was adapted from the procedure described by Nelson and Featherstone (1982). This method (method 1) was used to synthesize samples of pure HAP and AsHAP, and five intermediate compositions in the solid-solution series. A sample of nearly pure AsHAP (~1% P) was also synthesized for ^{31}P NMR study only, effectively allowing characterization across the entire solid-solution series. For the pure HAP, 50 mL of 0.19 *M* KH_2PO_4 with 0.1 *M* KNO_3 as a background electrolyte was added dropwise using a syringe pump at a precalibrated rate (0.25 mL/min) into 50 mL of a 0.21 *M* $Ca(NO_3)_2$ solution with 0.1 *M* KNO_3, which was kept at 75–80 °C over the duration of the experiment. The solution pH was maintained at 10.0 using an autotitrator with 2 *N* KOH, with constant stirring using a polytetrafluoroethylene (PTFE) stir bar. White precipitate was observed to form following addition of phosphate from the syringe. Synthesis of AsHAP or HAP-AsHAP solid-solution samples differed only by replacement of the KH_2PO_4 in the syringe with KH_2AsO_4 or by mixtures of KH_2PO_4 and KH_2AsO_4. At the end of the experiments, precipitates were recovered by filtration through 0.22 µm polypropylene membrane filters, repeated washing in deionized water, and drying in an oven at 60 °C. No further processing or annealing of the samples was performed. The fine, white powders were characterized by preliminary X-ray diffraction (XRD) to confirm formation of single-phase samples consistent with the peak positions for hydroxylapatite, johnbaumite (AsHAP) (Dunn et al. 1980), or positions intermediate between the end-members.

Two synthesis experiments (for pure AsHAP) were conducted following the same procedure (method 1) at ambient temperature (ca. 22 °C) and at 40 °C. XRD showed patterns typical of an amorphous phase, characterized by broad diffuse features (Fig. 1).

A limited number of pure AsHAP samples were synthesized at ambient temperature and at 90 °C using a second method (method 2), adapted from that described by Myneni et al. (1998). For room-temperature syntheses, 0.8 g of high-purity reagent CaO (Sigma-Aldrich, 99.995%, surface area 22 m^2/g) was placed into a 250 mL PTFE vessel, and 200 mL of 72 *mM* Na_2HAsO_4 solution (prepared from $Na_2HAsO_4 \cdot 7H_2O$; Sigma-Aldrich) were added to yield a 1 g/L suspension with initial pH 11.5. The suspension was agitated at room temperature, open to air, for 24 h. Final suspension pH was ~12. A similar procedure was used for sample synthesis at 90 °C, the differences being that reaction tubes were sealed within a pure nitrogen gas glovebox and then placed into a temperature-controlled oven at 90 ± 1 °C for 24 h. At the conclusions of the synthesis experiments, precipitates were recovered as described above, and XRD confirmed formation of single-phase johnbaumite.

Fourier transform infrared spectroscopy

FTIR spectra were obtained for all samples using a Thermo Nicolet Nexus 670 FTIR spectrometer equipped with an HgCdTe detector. Samples were mixed with KBr in uniform proportions and backgrounds were subtracted using a spectrum from a KBr blank. FTIR spectra were obtained by averaging 200 scans collected in diffuse reflectance mode from 4000 to 650 cm^{-1}, with 1 cm^{-1} resolution.

NMR spectroscopy

$^{31}P\{^1H\}$ CP/MAS NMR spectra were collected on a 400 MHz Varian Inova spectrometer (9.4 T) at operating frequencies of 161.8 and 399.8 MHz for ^{31}P and ^{1}H, respectively. We used a Varian/Chemagnetics T3-type probe assembly, with samples contained in 3.2 mm (o.d.) thin wall ZrO_2 rotors. The acquisition conditions for $^{31}P\{^1H\}$ CP/MAS experiments include a 5 kHz spinning rate and 5 ms contact time, with the transverse ^{31}P field (γB_1) ramped and centered near the first sideband match. Proton decoupling was employed during acquisition of all $^{31}P\{^1H\}$ CP/MAS spectra. The ^{31}P chemical shifts are reported relative to external

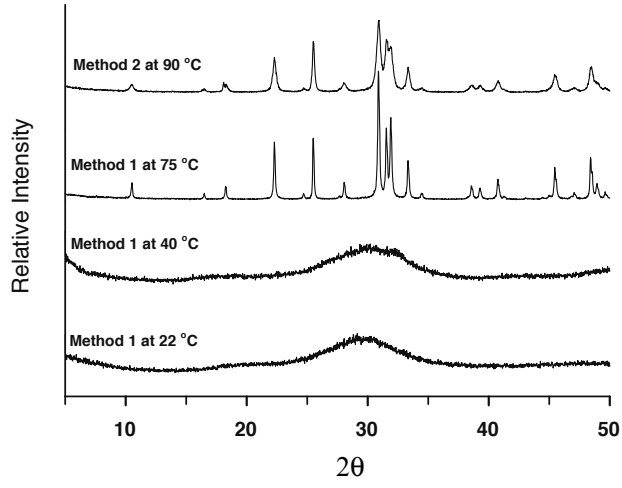

Figure 1. XRD scans (Cu*K*α) of products from two methods used for synthesizing $Ca_5(AsO_4)_3OH$ (AsHAP) at various temperatures. The two bottom scans are scaled differently from the top scans.

85% H_3PO_4 solution, using hydroxylapatite as a secondary reference set to δ_P = 2.65 ppm. ^{1}H MAS/NMR spectra were obtained with a Varian Chemagnetics Infinity plus spectrometer operating at 500 MHz and a spinning rate of 8 kHz. The ^{1}H chemical shifts are referenced to tetramethylsilane by setting the hydroxyl resonance of reagent grade hydroxylapatite to 0.2 ppm.

Powder X-ray diffraction and structure refinement methods

Preliminary powder XRD data were collected on a Scintag diffractometer (Bragg-Brentano geometry) over the range 5–75 °2θ using Cu$K\alpha$ radiation and a Ge solid-state detector. The sample was held in a flat cavity mount. Although satisfactory for confirming that sample products were single phase, the data were not satisfactory for structure refinement.

Powder XRD data were subsequently collected at the X16C beamline of the National Synchrotron Light Source, Brookhaven National Laboratory, Upton, New York, at a wavelength of 0.69707(1) Å for pure HAP and AsHAP and 0.69850(2) Å for the other samples, with a Ge(111) crystal analyzer and NaI scintillation detector. Samples were loaded into Lindemann glass capillaries of 1 mm nominal diameter, which were spun during data collection, carried out at ambient temperature. Patterns were collected in steps of 0.01° over the range 2–45°, with an average counting time of 10 s per step. Intensities were normalized to the signal from an ion chamber upstream of the sample. Each pattern was analyzed by the Rietveld method in space group $P6_3/m$ using Topas software (Bruker AXS 2005; Coelho 2000), including a phenomenological model for anisotropic strain broadening (Stephens 1999). A single isotropic displacement parameter, B, was refined for all atoms. No restraints were applied in the fits, although the hydroxyl hydrogen atom was omitted.

Extended X-ray absorption fine structure (EXAFS) spectroscopy

Arsenic *K*-edge EXAFS data were collected in transmission mode at beamline X11A of the National Synchrotron Light Source for AsHAP and AsO_4-substituted HAP samples. Samples were mixed with boron nitride in proportions required to obtain an edge step of $\Delta\mu x$ = 1–1.5. Absorption was measured using gas-filled ion chambers. A gold metal foil (L_{III}-edge 11918.7 eV) was used for energy calibration of the Si(111) monochromator. The second crystal of the monochromator was detuned by 20% to minimize harmonic contributions. Data processing was performed with the EXAFS data analysis program WinXAS (Ressler 1997). The EXAFS function was extracted using a cubic spline. The $\chi(k)$ function was Fourier transformed using k^3 weighting, and shell-by-shell fitting was done in *R*-space. Theoretical phases and amplitudes were calculated using FEFF7 (Zabinsky et al. 1995) for a johnbaumite structure model.

Thermogravimetric analysis (TGA)

Weight loss measurements were made for HAP, AsHAP, and one intermediate solid-solution sample using a Netzsch Jupiter STA 449 instrument with N_2 as the purge gas. The heating range was 30–1200 °C, with a heating rate of 10°/min.

Results and discussion

Solid-solution samples were synthesized for the nominal compositions listed in Table 1. Samples are designated by the percentage of As substitution (e.g., As43 has the As:P ratio of 43:57; As100 = AsHAP). A small portion of each synthesis product was dissolved in concentrated HNO_3 and analyzed by DCP (directly coupled plasma spectrophotometry) using appropriate standards. Analyzed Ca, P, and As ratios were found to differ slightly from nominal solution values as well as from values determined by refinement as described below.

Table 1. Compositional data for $Ca_5(P_xAs_{1-x}O_4)_3OH$ solid-solution samples

Sample designation	As:P in growth solution	As:P by DCP analysis	As:P by structure refinement
As100	100:0	100:0	100:0
As80	85:15	82:18	80:20
As66	70:30	68:32	66:34
As43	50:50	47:53	43:57
As24	30:70	30:70	24:76
As11	15:85	11:89	11:89
As0	0:100	0:100	0:100

Notes: Samples synthesized using method 1 at 75 °C. As100 is AsHAP (johnbaumite); As0 is HAP. As:P given in molar proportions.

FTIR spectra

FTIR spectra of the HAP-AsHAP samples are shown in Figure 2a. Spectra for the AsHAP samples synthesized using the $Ca(OH)_2$ method at 25 and 90 °C (not shown) are generally similar to that for the AsHAP shown in Figure 2a. Prominent bands at approximately 880–830 cm^{-1} are attributable to the ν_3-stretching modes of the AsO_4^{3-} groups, and are consistent with the IR spectra shown by Massuyes et al. (1969) and Kusachi et al. (1996) for synthetic AsHAP and natural johnbaumite samples, respectively, as well as with the positions reported by Myneni et al. (1998) for synthetic AsHAP. The FTIR spectrum for pure HAP shows the corresponding ν_3 modes for PO_4^{3-} groups at 1100–1030 cm^{-1}, and is consistent with other reported spectra for synthetic HAP. Spectra of samples at intermediate compositions show distinct ν_3 modes for both AsO_4^{3-} and PO_4^{3-} groups, with progressive changes in overall intensity corresponding to As and P contents. However, positions of these modes remain largely unchanged across the solid solution. This two-mode behavior suggests little interaction between P- and As-centered tetrahedra.

Broad absorption is evident over the range 3600–2700 cm^{-1} in all spectra and likely reflects the presence of H_2O. An OH-bending mode associated with bound water is evident at ~1650 cm^{-1} in all spectra. The sharp feature at ~3565 cm^{-1} is attributed to an OH stretch. The position of this peak changes progressively with As substitution, from 3571 cm^{-1} in HAP to 3560 cm^{-1} in pure AsHAP (Fig. 2b).

Absorption bands at ~1455–1410 cm^{-1} indicate the presence of carbonate (ν_3, asymmetric stretching mode) in all samples (Fig. 3). The ν_2-bending mode of CO_3 is also present in the HAP spectrum at 873 cm^{-1}, but is obscured in all of the AsO_4-containing samples by the prominent ν_3 As-O-stretching modes. In HAP, carbonate substitution is known to occur in OH sites (type A) and PO_4 sites (type B), with both substitutions occurring in some samples (LeGeros et al. 1969). Most researchers have concluded that carbonate substitution occurs dominantly in PO_4 sites (type B) in HAP grown from low-temperature solutions (cf. Wopenka and Pasteris 2005). There has been considerable work addressing IR spectral characteristics that can be used to distinguish substitution type. Doublet peaks in the ν_3 mode at ~1535 and ~1463 cm^{-1} have normally been assigned to type A carbonate, whereas doublet peaks at ~1456 and ~1422 cm^{-1} have been interpreted as type B carbonate (Rey et al. 1989; but also see Fleet and Liu 2004, and Wilson et al. 2006). In the HAP spectrum, we observe doublet peaks at ~1451 and 1419 cm^{-1}, which is consistent with type B carbonate. In the solid-solution samples, the same ν_3 doublet is observed, but the peak positions shift to higher and lower wave numbers, resulting in greater splitting with increasing AsO_4 content (Fig. 3).

Thermogravimetric analysis

Weight loss curves for HAP, AsHAP, and the As43 solid solution are similar in shape but offset slightly (Fig. 4). All samples show 2–3% weight loss upon heating from ambient temperature

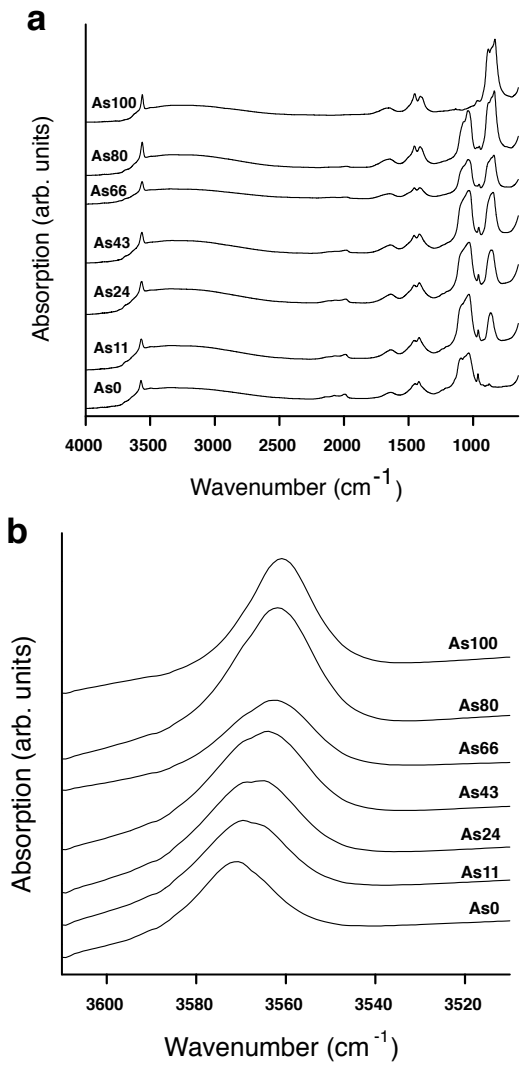

FIGURE 2. (**a**) FTIR spectra of method 1 samples of the HAP-AsHAP solid solution. Sample labels indicate percentage of As substitution as determined by structure refinement. (**b**) Expanded view showing the region with the sharp feature interpreted as OH stretching.

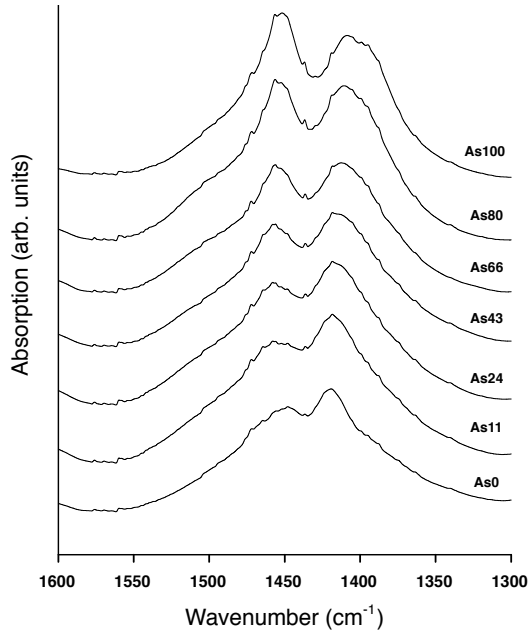

FIGURE 3. FTIR spectra of HAP-AsHAP samples showing peaks attributable to carbonate substitution. Sample labels indicate percentage of As substitution as determined by structure refinement.

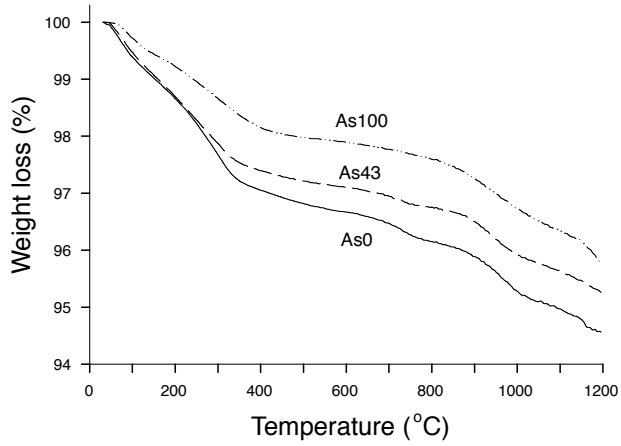

FIGURE 4. Weight loss curves from thermogravimetric analysis of AsHAP (As100), HAP (As0), and an intermediate solid solution (As43).

to ~500 °C. This is attributed to loss of adsorbed and structural H_2O. The rate of weight loss is lower in the interval from ~500 to 700 °C, followed by an interval of increased weight loss up to 1000 °C, with some weight loss continues through 1200 °C. Loss of CO_3 in synthetic carbonate-containing HAP is reported to occur over the temperature range 550–1000 °C, with most loss occurring at 700–950 °C (Elliott 1994; Mayer et al. 1997; Ivanova et al. 2001; Krajewski et al. 2005). The weight losses observed for our samples over the range 550–1000 °C are 1.2–1.5%, or ~2% if this range is extended to 1200 °C, and are likely due to loss of CO_2. These results indicate that small and similar amounts of CO_3 are present in the samples spanning the solid solution.

X-ray diffraction and structure refinements

Figure 5 shows a portion of the powder X-ray diffraction pattern of each of the seven samples. It is clear that each of the samples is phase-pure, and their diffraction lines show a progressive shift across the entire range of solid solutions. No evidence was observed for splitting of peaks that would indicate monoclinic or triclinic symmetry. Rietveld refinements were performed in space group $P6_3/m$ and results are summarized in Table 2. Comparisons of raw data and fits are shown for As100 (AsHAP) and As43 samples in Figure 6. Complete refinement data and the raw and refined profiles are available as Supplementary information[1]. No account was taken in the refinements

[1] Deposit item AM-09-028, Supplemental Information. Deposit items are available two ways: For a paper copy contact the Business Office of the Mineralogical Society of America (see inside front cover of recent issue) for price information. For an electronic copy visit the MSA web site at http://www.minsocam.org, go to the American Mineralogist Contents, find the table of contents for the specific volume/issue wanted, and then click on the deposit link there.

for hydroxyl H-atoms or the small amount of carbonate observed from FTIR. The refined As occupancies for two intermediate composition samples (As24; As43) are less than values determined by DCP analysis by several percent (Table 1), which we attribute to dilution errors during acidification or presence of poorly crystalline impurities, evidence for which is observed in NMR spectra (below). We consider the refined occupancy values to be more reliable.

The unit-cell parameters and cell volume increase smoothly with increasing As content (Fig. 7). The *a* cell parameter is more sensitive than *c* to substitution on the B site, as also found by Mercier et al. (2007) for V substitution for P in fluorapatite. The individual B-O distances in the averaged As,P tetrahedra increase with increasing As content, as expected (Fig. 8). However, the (As,P)-O1 distance increases more rapidly with increasing As content until approximately 2/3 occupancy, after which no further change is observed, indicating a greater distortion in the averaged tetrahedra for intermediate compositions. Ca1-O and Ca2-O distances (Fig. 9) exhibit relatively small or no changes with As substitution. Therefore, expansion of the unit cell in response to AsO_4 substitution is primarily a result of an average expansion of the BO_4 tetrahedra.

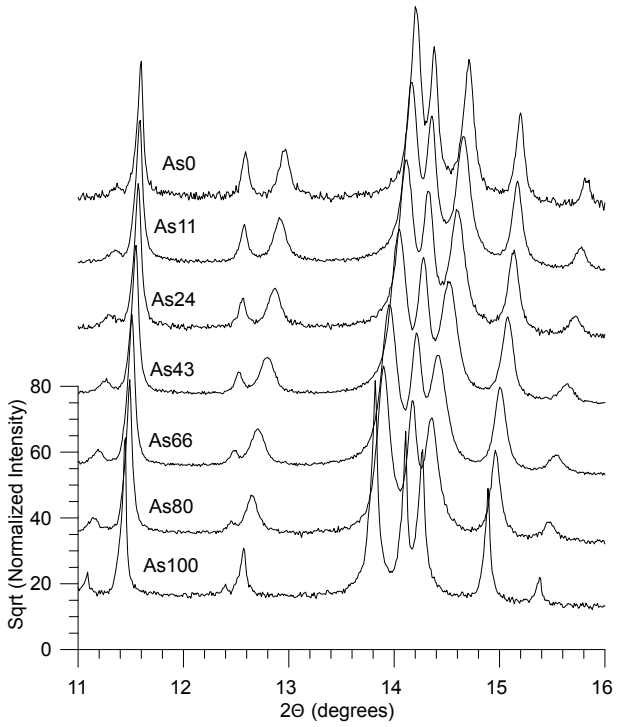

FIGURE 5. Partial powder synchrotron X-ray diffraction patterns of all seven samples.

Replacement of PO_4 by larger tetrahedra, such as AsO_4 and VO_4, has the effect of increasing separation between Ca1 polyhedra, in which the six nearest oxygen atoms form metaprisms that compose the ring-like A1-BO_4 framework. The dilation of this ring-like framework, which lies perpendicular to **c**, explains the greater sensitivity of the *a* cell parameter to substitution of As for P. Mercier et al. (2007) examined V substitution for P in fluorapatite, and demonstrated that the V,P tetrahedra also tilt as the average (V,P)-O distance increases with increasing V content, accompanied by slight increases in Ca1-O bond length. At highest V contents, the symmetry is reduced from the $P6_3/m$ observed for the P-rich fluorapatite samples. Baikie et al. (2007) showed that limitations to expansion of the A1-BO_4 framework imposed by the A2-X tunnel components cause the tetrahedra to undergo tilting that lowers the symmetry to triclinic. This was also observed in $Ca_5(AsO_4)_3F$ and in $Cd_5(PO_4)_3F$ (Kreidler and Hummel 1970; Baikie et al. 2007). In the former case, the size of the B cation is increased relative to that in $Ca_5(PO_4)_3F$, and in the latter case the size of the A cation is decreased relative to that in $Ca_5(PO_4)_3F$.

Being aware of the potential for similar reduction of symmetry for the As-rich samples in the present work, and yet having failed to see any clear evidence to support lower symmetry, we carried out a refinement of the As100 sample in space group $P\bar{1}$ using positional parameters from triclinic $Ca_5(AsO_4)_3F$ as a starting model (Baikie et al. 2007). The unit cell refined to values that are indistinguishable within standard errors from hexagonal values, and no improvement in fit was obtained. Calculated positions for diffraction peaks that would split as a result of triclinic distortion were so close to one another that they would not be distinguishable from our synchrotron data.

Expansion of the average size of As,P tetrahedra is also reflected in the widely considered metaprism twist angle, φ, giving the rotation of the two triangular faces formed by O1 and O2 about Ca1 (Fig. 10) (White and Dong 2003). This angle varies inversely according to the relative sizes of the A1-BO_4 and the A2-X constituents. For example, nearly a 10° variation in the metaprism twist angle has been observed across a series of Ca apatites (White and Dong 2003). On the other hand Mercier et al. (2007) found a relatively small variation of the twist angle (<2°) for substitution of P by V in a series of $Ca_5(V_xP_{1-x}O_4)_3F$ apatites. The variation in the twist angle, φ, with average size of the tetrahedral B ion in the present solid-solution series is shown in Figure 10, with values listed in Table 2. The trend is

TABLE 2. Results of Rietveld structure refinements

	As100	As80	As66	As43	As24	As11	As0
As frac	1	0.802(5)	0.657(4)	0.433(4)	0.242(4)	0.110(2)	0
a (Å)	9.7156(2)	9.6758(3)	9.6311(3)	9.5640(3)	9.5075(3)	9.4655(3)	9.4212(3)
c (Å)	6.9857(1)	6.9732(2)	6.9556(2)	6.9360(2)	6.9187(2)	6.9068(2)	6.8927(2)
V (Å^3)	571.05(3)	565.35(3)	558.73(3)	549.42(3)	541.59(3)	535.89(3)	529.81(3)
Average (As,P)-O (Å)	1.697(4)	1.662(3)	1.649(3)	1.606(3)	1.576(3)	1.550(2)	1.541(4)
φ_{twist} (°)	23.5(3)	25.5(3)	25.9(3)	25.5(3)	25.4(3)	24.5(2)	23.6(3)
R_{wp} (%)	7.05	6.38	6.33	6.03	6.96	5.19	8.96
R_{exp} (%)	3.43	4.00	2.88	2.80	5.18	2.70	7.51
χ^2	4.23	2.55	4.82	4.64	1.81	3.69	1.42

Notes: As100 is AsHAP (johnbaumite); As0 is HAP. Numbers in parentheses are standard uncertainties computed by the least-squares Rietveld fit. As such, they represent statistical precision propagated from the counting statistics. A realistic estimate of the experimental accuracy would be several times larger.

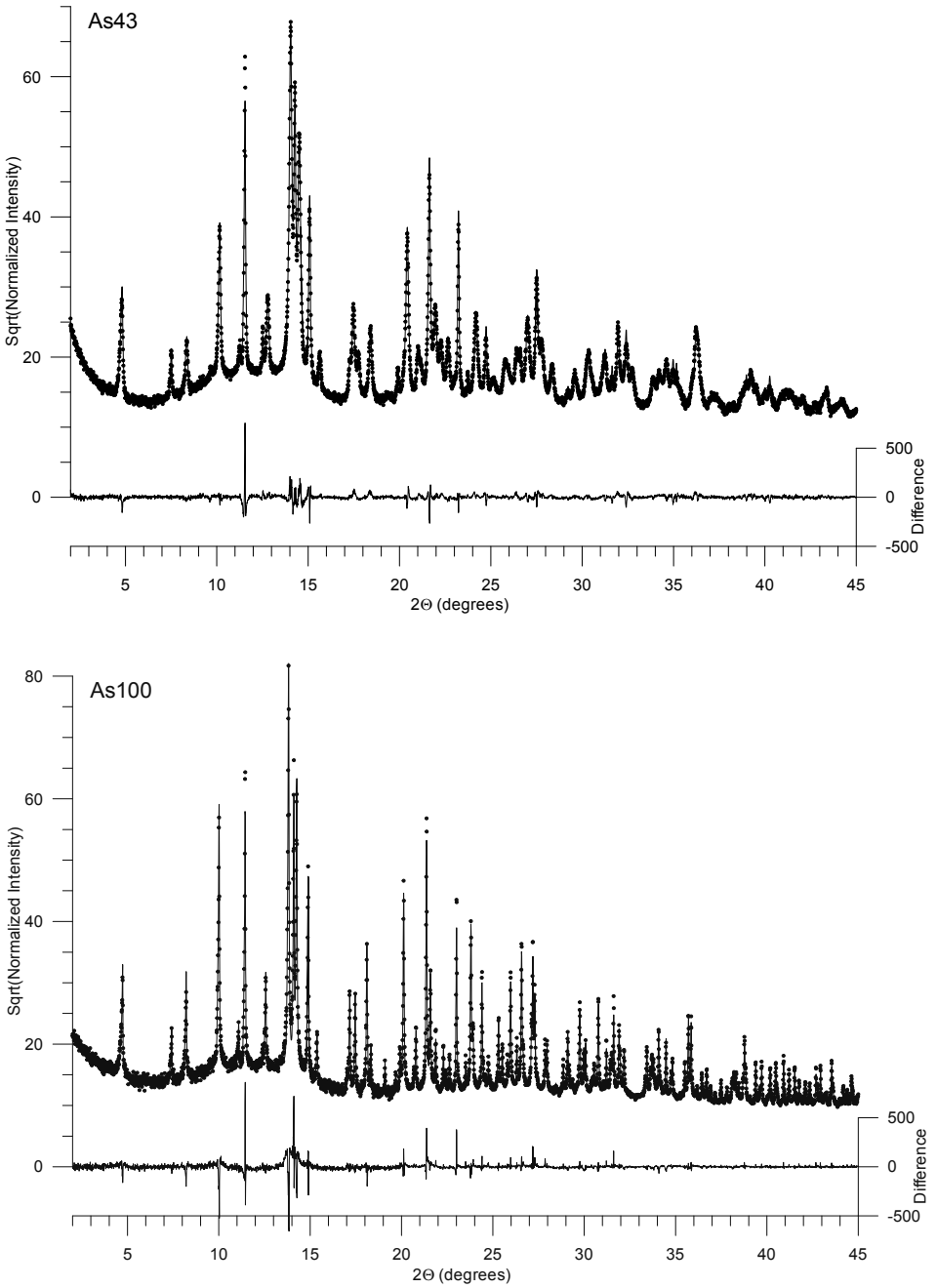

FIGURE 6. Raw X-ray data (solid dots) and Rietveld refinement fits (line) for As43 (top) and As100 (bottom) samples. Raw data and fit are shown on a square-root scale to increase visible dynamic range. The residual (data minus model) is shown on a linear scale.

asymmetric parabolic, with a maximum variation of 2.4(3)°. The trend of increasing twist with increasing As content up to As fraction 0.66 is consistent with the above explanation. We cannot explain the decrease in twist angle at higher As values. We note, however, that the observed trend is consistent with the distortion between the (As,P)-O distances (Fig. 8), where the (As,P)-O1 distance increases more rapidly than the (As,P)-O2 distance over the intermediate concentration range, which would serve to accentuate the metaprism twist in this same range, as is observed.

In the structure refinements, we ignored the small amount of CO_3 shown to be present, focusing instead on the influence of As substitution. We cannot rule out the possibility that the presence of CO_3 may affect some of the trends that we have described, including that for the metaprism twist angle. However, the low CO_3 contents (<2 wt%), and the similar amounts for the three samples examined by TGA, would suggest that any such effect is likely to be small.

EXAFS

Inasmuch as EXAFS is element specific, the As *K*-edge EXAFS results allow us to compare the As-O distances with

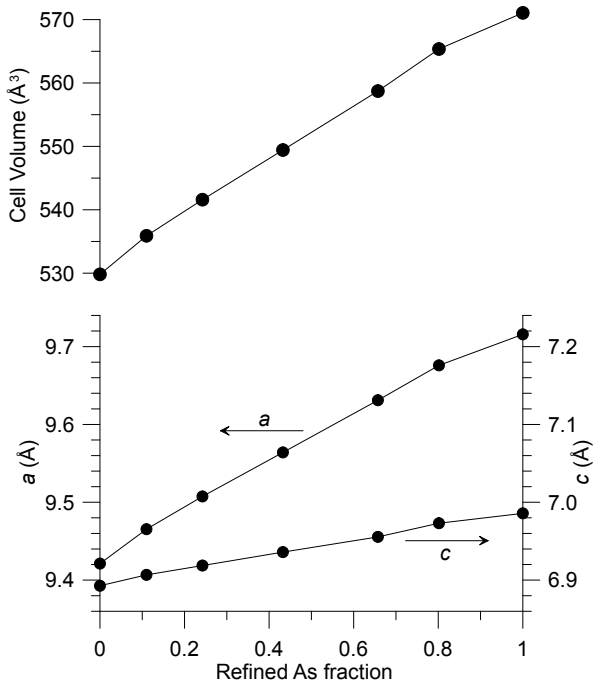

FIGURE 7. Unit-cell parameters and cell volume as a function of the refined As fraction. Errors are within the size of the symbols. Lines are provided for ease of viewing.

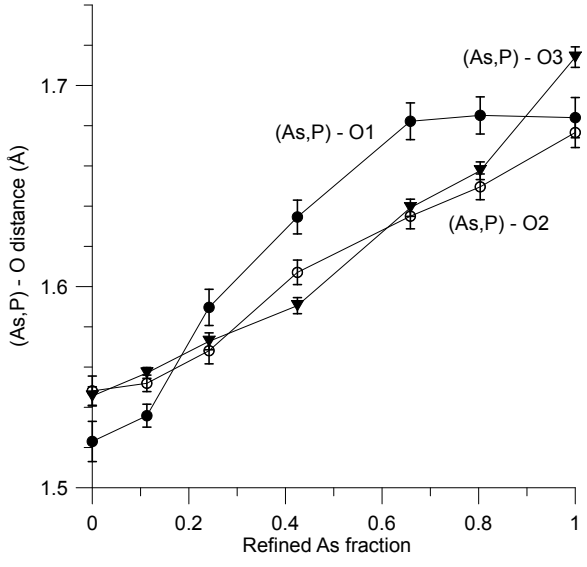

FIGURE 8. Refined (As,P)-O distances in the (As,P) tetrahedra as a function of refined As fraction. Lines are provided for ease of viewing.

the average tetrahedral B-O distances determined by Rietveld refinement, which show a progressive growth with increasing As substitution (Fig. 8). The separation among the different As-O distances in the AsO_4 tetrahedron is too small to distinguish in the EXAFS, so that a single oxygen shell was fit. Two calcium shells were also fit. Figure 11 shows EXAFS chi functions and corresponding Fourier transform (FT) magnitudes for the six AsO_4-containing samples. Fit results are given in Table 3. EX-

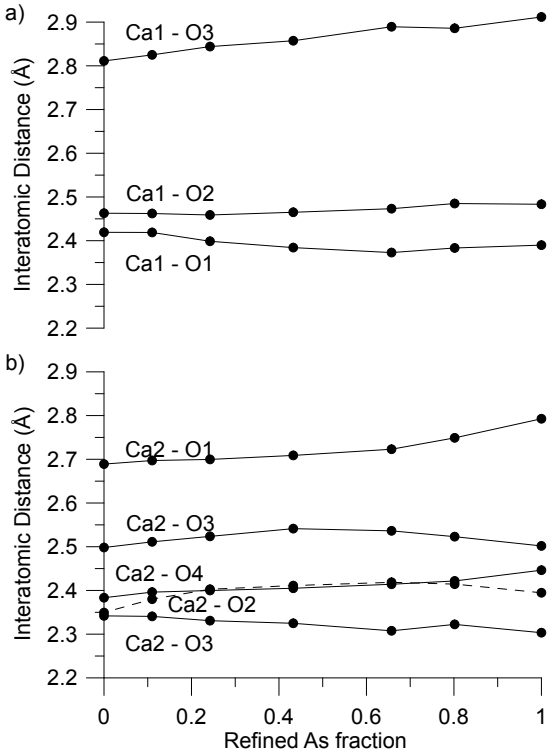

FIGURE 9. Ca-O distances for the (**a**) Ca1 and (**b**) Ca2 sites as a function of refined As fraction. Errors are within the size of the symbols. Lines are provided for ease of viewing.

AFS chi curves and FT magnitudes are nearly identical for all samples, indicating that the local environment of As is essentially the same in all samples. The fit results confirm that the average As-O distance (As-O = 1.68 ± 0.01 Å) remains unchanged in all samples. Fitted distances to Ca shells are largely similar among the samples. As is understood from studies in other solid solutions, the As-O distance is conserved, and the smooth variation in B-O distance observed from structure refinements reflects the statistical average of As-O and P-O distances.

NMR spectroscopy

The $^{31}P\{^{1}H\}$ CP/MAS NMR spectra of samples along the HAP-AsHAP series (Fig. 12) reveal a smooth variation in the average local P environment. The HAP end-member yields a symmetrical, relatively narrow ^{31}P NMR peak, 1.3 ppm full-width at half maximum (FWHM), at a chemical shift of δ_P = +2.65 ppm that is identical to previous reports. The occurrence of an additional small peak near +7 ppm suggests the presence of a minor amount of an unidentified impurity; a shoulder at a similar chemical shift was also noted for the As-containing samples. With increasing arsenate content the ^{31}P NMR peak occurs at increasingly higher chemical shifts and broadens. For both peak width and position, the variation is nonlinear with mole fraction of phosphate, displaying a distinct sigmoidal curvature. An additional sample with a small amount of phosphate (1%) was prepared for NMR analysis to complete the trend toward the AsHAP end-member, which gives a chemical shift of δ_P = +3.65 ppm and a width of 2.2 ppm (FWHM). Attempts to obtain useful

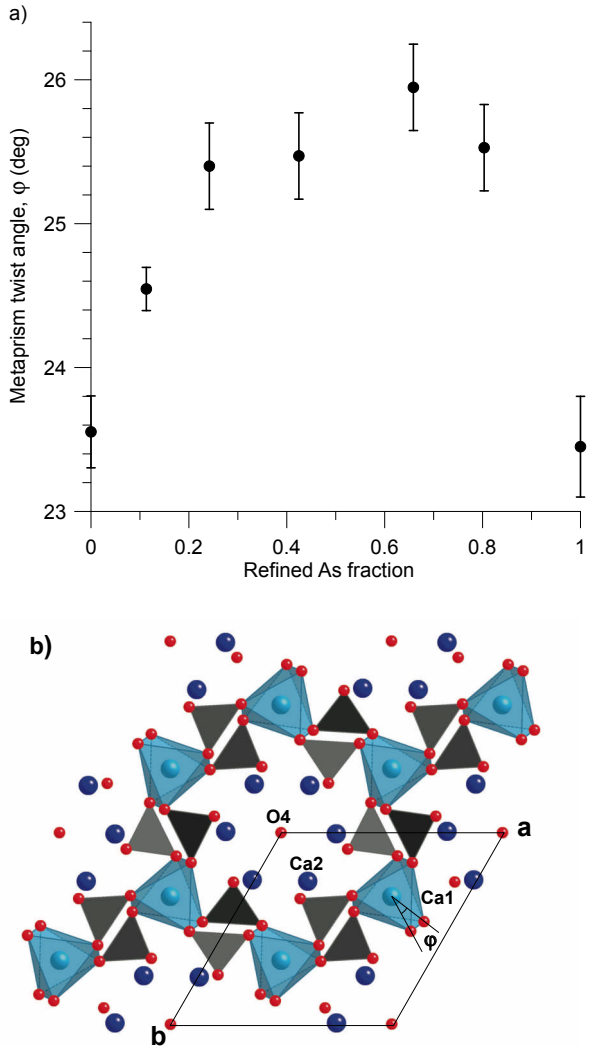

FIGURE 10. (**a**) Metaprism twist angle, φ, as a function of refined As fraction. (**b**) View of HAP structure looking down [0001], showing the metaprism twist angle, φ, which relates triangles formed by O1 and O2 atoms. Ca1 sites shown as metaprisms; Ca2 shown as spheres.

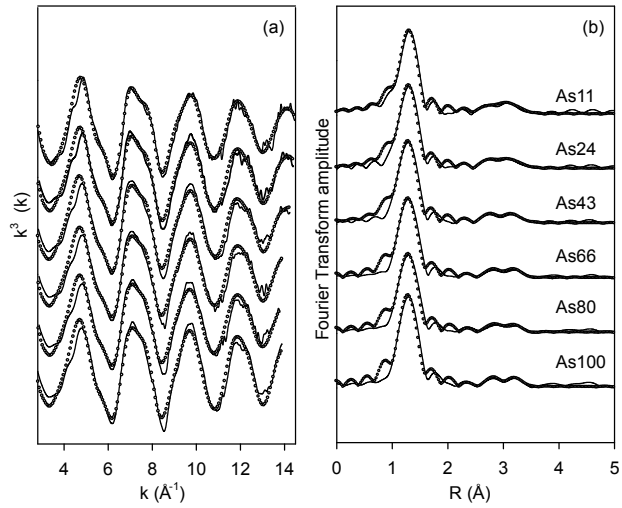

FIGURE 11. (**a**) k^3-weighted EXAFS and (**b**) corresponding Fourier transform amplitudes for AsHAP and AsO_4-substituted HAP samples, showing experimental data (solid lines) and fits (open circles).

TABLE 3. EXAFS fitting results for $Ca_5(P_xAs_{1-x}O_4)_3OH$ solid-solution samples

Sample	Shell	CN	*R* (Å)	σ² (Å²)*	E_0 (eV)	Residual(%)†
As100	As-O	4.5	1.68	0.001	2.62	14.3
	As-Ca	0.3	3.19	0.001		
	As-Ca	3.3	3.64	0.009		
As80	As-O	4.2	1.68	0.002	3.49	16.6
	As-Ca	0.6	3.20	0.005		
	As-Ca	3.6	3.64	0.01		
As66	As-O	4.2	1.68	0.002	2.59	15.9
	As-Ca	0.3	3.20	0.001		
	As-Ca	3.2	3.64	0.009		
As43	As-O	4.6	1.67	0.002	1.83	14.9
	As-Ca	0.4	3.18	0.001		
	As-Ca	3.2	3.63	0.008		
As24	As-O	4.3	1.68	0.002	3.26	13.1
	As-Ca	0.7	3.19	0.004		
	As-Ca	3.7	3.63	0.009		
As11	As-O	4.4	1.68	0.002	10.22	5.8
	As-Ca	1.6	3.21	0.008		
	As-Ca	3.7	3.64	0.009		

Notes: S_0^2 value fixed at 1. Estimated errors are CN = ±20%; *R* = ±0.01 Å for first shell, ±0.05 Å for higher shells; Debye-Waller factor = ±0.001 Å² for first shell, ±0.005 Å² for higher shells.
* Debye-Waller type factor.

$$\dagger \text{Residual}(\%) = \sum_{i=1}^{N} |y_{exp}(i) - y_{theo}(i)| \Big/ \sum_{i=1}^{N} |y_{exp}(i)| \times 100$$

with *N* the number of data points, y_{exp} and y_{theo} experimental and theoretical data points, respectively.

^{75}As NMR spectra were not successful. Symmetrical peaks were observed for all compositions, which indicates absence of any significant anion clustering into HAP-like domains. Although the chemical shift variation across the series is small (~1 ppm), the presence of phosphate-rich clusters would be expected to yield a shoulder or asymmetry toward the peak position for HAP, because the NMR chemical shifts depend only on short-range atomic configurations.

In contrast to the As EXAFS results, these NMR data indicate some changes in the local structure of the phosphate tetrahedra with As/P ratio across the solid-solution series. However, previously reported correlations of ^{31}P chemical shifts with structural data suggest that very small changes in bond length could account for these observations. For example, Cheetham et al. (1986) relate variations in δ_P to the sum of the bond strengths to the phosphate O atoms. The +1 ppm change in δ_P from As0 to As99 corresponds to a decrease in bond strength sum of less than 0.02, which can result from an increase in the average P-O distance of less than 0.002 Å. ^{31}P chemical shifts are expected to depend also on pi bond order (e.g., Sternberg et al. 1990), so variations in the P-O-Ca angles could also effect δ_P. Nonetheless, the form of the ^{31}P chemical shift variation with composition does not resemble those for any of the cell dimensions or average structure parameters, including metaprism twist angle. Combined with the distribution of δ_P implied by the increase in ^{31}P peak width with increasing As content, this result suggests that variations in local configuration are accommodated within the average structure.

The ^{1}H MAS/NMR spectra of all samples (not shown) contain a relatively narrow peak at $\delta_H = 0.2$ ppm for the apatite hydroxyl

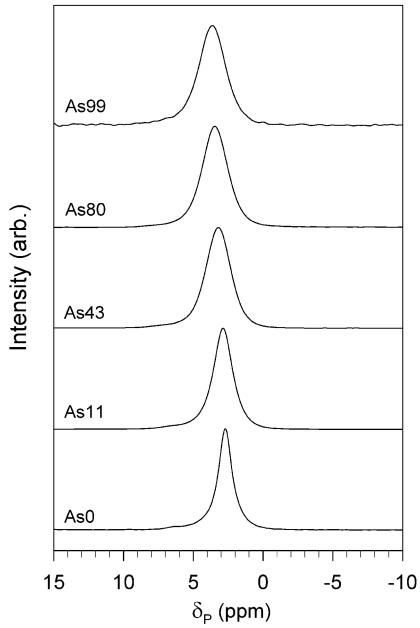

FIGURE 12. $^{31}P\{^{1}H\}$ CP/MAS NMR spectra of samples along the HAP-AsHAP series. Data obtained with 5 ms contact time and 2 s relaxation delay at spinning rate of 5 kHz.

group plus a broader peak due to water at 5.7 ppm, with similar integrated intensities. This latter peak resembles that observed for disordered surface regions of nanocrystalline HAP (Jager et al. 2006). The presence of a resonance for water from all of the HAP-AsHAP samples is consistent with the low-temperature weight loss in TGA traces and the presence of a broad 3600–2700 cm^{-1} absorption and water bending modes in FTIR spectra. Within experimental error (ca. ±0.05 ppm), we find no systematic change in the ^{1}H chemical shift of the hydroxyl resonance with As content, in contrast to the small systematic change in the corresponding OH-stretching frequency.

CONCLUDING REMARKS

Although the present structural results demonstrate generally uniform and progressive changes in most structure parameters as a result of As substitution in HAP, distortion in the BO_4 tetrahedra over the intermediate composition range—also expressed in the metaprism twist angle—is not explained. Furthermore, clustering of PO_4 tetrahedra can be ruled out on the basis of NMR results. The lack of any evidence to suggest lowering of symmetry in As-rich samples may be reason to investigate samples synthesized under different conditions, including at higher synthesis temperatures. Beyond these structural considerations, the progressive and predictable variation of the structure in this solid-solution series suggests that formation of compositionally diverse samples should be expected.

ACKNOWLEDGMENTS

We thank Tim White for especially useful comments and a review. Y.J.L. was supported by the Korean Research Foundation Grant funded by the Korean Government (KRF-2007-331-C00250) and also partially supported by Korean University Grant. Support was also provided by the Center for Environmental Molecular Science (NSF CHE-0221934). Use of the National Synchrotron Light Source, Brookhaven National Laboratory, was supported by the U.S. Department of Energy, Office of Science, Office of Basic Energy Sciences, under contract no. DE-AC02-98CH10886. We thank beamline personnel at X11A for assistance.

REFERENCES CITED

Baikie, T., Mercier, P.H.J., Elcombe, M.M., Kim, J.Y., Le Page, Y., Mitchell, L.D., White, T.J., and Whitfield, P.S. (2007) Triclinic apatites. Acta Crystallographica, B63, 251–263.

Bothe, J.V. and Brown, P.W. (1999a) Arsenic immobilization by calcium arsenate formation. Environmental Science and Technology, 33, 3806–3811.

——— (1999b) The stabilities of calcium arsenates at 23 ± 1 °C. Journal of Hazardous Materials, B69, 197–207.

Bruker AXS (2005) TOPAS V3: General profile and structure analysis software for powder diffraction data. User's Manual, Bruker AXS, Karlsruhe, Germany.

Cheetham, A.K., Clayden, N.J., Dobson, C.M., and Jakeman, R.J.B. (1986) Correlations between ^{31}P NMR chemical shifts and structural parameters in crystalline inorganic phosphates. Journal of the Chemical Society Chemical Communications, 195–197.

Choong, T.S.Y., Chuah, T.G., Robiah, Y., Koay, F.L.G., and Azni, I. (2007) Arsenic toxicity, health hazards and removal techniques from water: An overview. Desalination, 217, 139–166.

Coelho, A.A. (2000) Whole-profile structure solution from powder diffraction data using simulated annealing. Journal of Applied Crystallography, 33, 899–908.

Donahue, R. and Hendry, M.J. (2003) Geochemistry of arsenic in uranium mine tailings, Saskatchewan, Canada. Applied Geochemistry, 18, 1733–1750.

Dunn, P.J., Peacor, D.R., and Newberry, N. (1980) Johnbaumite, a new member of the apatite group from Franklin, New Jersey. American Mineralogist, 65, 1143–1145.

Elliott, J.C. (1994) Structure and Chemistry of the Apatites and Other Calcium Orthophosphates, Vol. 18. Studies in Inorganic Chemistry, Elsevier, Amsterdam.

Fleet, M.E. and Liu, X. (2004) Location of type B carbonate in type A-B carbonate apatite synthesized at high pressure. Journal of Solid State Chemistry, 177, 3174–3182.

George, G., Gupta, S.K., Rao, P.V.R., and Narasaraju, T.S.B. (1987) Preparation and characterization of phosphate and arsenate apatites of strontium and their solid solutions. Journal of Materials Science, 22, 2274–2276.

Ivanova, T.I., Frank-Kamenetskaya, O.V., Kol'tsov, A.B., and Ugolkov, V.L. (2001) Crystal structure of calcium-deficient carbonated hydroxyapatite. Journal of Solid State Chemistry, 160, 340–349.

Jager, C., Welzel, T., Meyer-Zaika, W., and Epple, M. (2006) A solid-state NMR investigation of the structure of nanocrystalline hydroxyapatite. Magnetic Resonance in Chemistry, 44, 573–580.

Krajewski, A., Mazzocchi, M., Buldini, P.L., Ravaglioli, A., Tinti, A., Taddei, P., and Fagnano, C. (2005) Synthesis of carbonated hydroxyapatites: Efficiency of the substitution and critical evaluation of analytical methods. Journal of Molecular Structure, 744–747, 221–228.

Kreidler, E.R. and Hummel, F.A. (1970) The crystal chemistry of apatite: Structure fields of fluor- and chlorapatite. American Mineralogist, 55, 170–184.

Kusachi, I., Henmi, C., and Kobayashi, S. (1996) Johnbaumite from Fuka, Okayama Prefecture, Japan. Mineralogical Journal, 18, 60–66.

LeGeros, R.Z., Trautz, O.R., Klein, E., and LeGeros, J.P. (1969) Two types of carbonate substitution in the apatite structure. Experientia, 25, 5–7.

Magalhaes, M.C.F. and Williams, P.A. (2007) Apatite group minerals: Solubility and environmental remediation. In T.M. Letcher, Ed., Thermodynamics, Solubility and Environmental Issues, p. 327–340. Elsevier, Amsterdam.

Mahapatra, P.P., Mahapatra, L.M., and Mishra, B. (1987) Arsenate hydroxyapatite: A physico-chemical and thermodynamic investigation. Polyhedron, 6, 1049–1052.

Massuyes, M., Trombe, J.-C., Bonel, G., and Montel, G. (1969) Etude compare des structures et des proprietes physico-chimiques de quelques apatites calciques phospho-arseniees. Bulletin de la Societe Chimique de France, 7, 2308–2315.

Mayer, I., Schlam, R., and Featherstone, F.D.B. (1997) Magnesium-containing carbonate apatites. Journal of Inorganic Biochemistry, 66, 1–6.

Mercier, P.H.J., Dong, Z.L., Baikie, T., Le Page, Y., White, T.J., Whitfield, P.S., and Mitchel, L.D. (2007) Ab initio constrained crystal-chemical Rietveld refinement of $Ca_{10}(V_xP_{1-x}O_4)_6F_2$ apatites. Acta Crystallographica, B63, 37–48.

Mondal, P., Majumder, C.B., and Mohanty, B. (2006) Laboratory based approaches for arsenic remediation from contaminated water: Recent developments. Journal of Hazardous Materials, B137, 464–479.

Moon, D.H., Dermatas, D., and Menounou, N. (2004) Arsenic immobilization by calcium-arsenic precipitates in lime treated soils. Science of the Total Environment, 330, 171–185.

Myneni, S.C.B., Traina, S.J., Logan, T.J., and Waychunas, G.A. (1997) Oxyanion behavior in alkaline environments: Sorption and desorption of arsenate in etringite. Environmental Science and Technology, 31, 1761–1768.

Myneni, S.C.B., Traina, S.J., Waychunas, G.A., and Logan, T.J. (1998) Arsenate interactions with CaO: Formation of johnbaumite. Mineralogical Magazine,

62A, 1050–1051.
Nelson, D.G.A. and Featherstone, J.D.B. (1982) Preparation, analysis, and characterization of carbonated apatites. Calcified Tissue International, 34, S69–S81.
Nishimura, T. and Robins, R.G. (1998) A re-evaluation of the solubility and stability regions of calcium arsenites and calcium arsenates in aqueous solution at 25 °C. Mineral Processing and Extractive Metallurgy Review, 18, 283–308.
Ressler, T. (1997) WinXAS: A new software package not only for the analysis of energy-dispersive XAS data. Journal de Physique IV, 7, C2–269.
Rey, C., Collins, B., Goehl, T., Dickson, I.R., and Glimcher, M.J. (1989) The carbonate environment in bone mineral: A resolution-enhanced Fourier transform infrared spectroscopy study. Calcified Tissue International, 45, 157–164.
Robins, R.G. (1981) The solubility of metal arsenates. Metallurgical and Materials Transactions B, 12, 103–109.
——— (1985) The aqueous chemistry of arsenic in relation to hydrometallurgical processes. In A.J. Oliver, Ed., Impurity Control and Disposal, p. 1.1–1.26. Proceedings of the 15th Hydrometallurgy Symposium CIM, Vancouver.
Stephens, P.W. (1999) Phenomenological model of anisotropic peak broadening in powder diffraction. Journal of Applied Crystallography, 32, 281–289.
Sternberg, U., Pietrowski, F., and Priess, W. (1990) The influence of structure and coordination on the ^{31}P-chemical shift in phosphates. Zeitschrift für Physikalische Chemie, Neue Folge, 168, 115–128.
U.S. Environmental Protection Agency (1998) Final Report—Arsenic Stabilization Research Project; Mine Waste Technology Program Activity IV, Project 5. Montana Tech of The University of Montana and MSE Technology Applications, Inc., www.epa.gov/hardrockmining/a4/a4p5.pdf.
White, T.J. and Dong, Z.L. (2003) Structural derivation and crystal chemistry of apatites. Acta Crystallographica, B59, 1–16.
Wilson, R.M., Dowker, S.E.P., and Elliott, J.C. (2006) Rietveld refinements and spectroscopic structural studies of a Na-free carbonate apatite made by hydrolysis of monetite. Biomaterials, 27, 4682–4692.
Wopenka, B. and Pasteris, J.D. (2005) A mineralogical perspective on the apatite in bone. Materials Science and Engineering C, 25, 131–143.
Zabinsky, S.I., Rehr, J.J., Ankudinov, A., Albers, R.C., and Eller M.J. (1995) Multiple-scattering calculations of X-ray absorption spectra. Physical Review, B52, 2995–3009.
Zhu, Y.N., Zhang, X.H., Xie, Q.L., Wang, D.Q., and Cheng, G.W. (2006) Solubility and stability of calcium arsenates at 25 °C. Water, Air and Soil Pollution, 169, 221–238.

Manuscript received October 16, 2008
Manuscript accepted January 29, 2009
Manuscript handled by Hongwu Xu